

Determination of water vapor trends from VLBI observations



*Robert Heinkelmann, Michael Schmidt,
Johannes Böhm and Harald Schuh*

Abstract

Very Long Baseline Interferometry (VLBI) observations can be analyzed to derive precipitable water, which can be an important contribution for meteorological research. Since some of the VLBI stations observe for more than twenty years, it is possible to determine long-term trends. In this work we introduce two methods for the climate trend determination: the robust estimation of a linear trend using the bounded influence by standardized residuals (BIBER) – estimator, and a multi-resolution quadratic normalized B-spline wavelet model for the representation of linear and non-linear trend characteristics. If the trend is modeled by the wavelets instead of a solely linear term, the rms of the residuals becomes significantly smaller. Robust estimated linear trends of water vapor at twelve globally distributed VLBI sites are presented.

Kurzfassung

Beobachtungen der Radiointerferometrie auf langen Basislinien (VLBI) können zur Bestimmung des ausfällbaren Wassers in der Atmosphäre über den Messstationen herangezogen werden. Die Zeitreihen können einen wichtigen Beitrag für die meteorologische Forschung leisten. Da von manchen VLBI Stationen Beobachtungsreihen über mehr als zwanzig Jahre vorliegen, können langfristige Trends berechnet werden. In dieser Studie werden zwei Methoden zur Trendbestimmung untersucht: Zum einen werden lineare Trendanteile mit dem BIBER-Schätzer (bounded influence by standardized residuals) bestimmt, zum anderen werden lineare und nicht-lineare Eigenschaften der Trendkomponente mit normierten, quadratischen B-spline Wavelets dargestellt. Wird der Trendanteil im Gegensatz zu einem linearen Term durch die Wavelets beschrieben, so sind die Standardabweichungen der Residuen signifikant kleiner. Robust geschätzte lineare Trends an zwölf global verteilten VLBI Stationen werden präsentiert.

1. Introduction

Water vapor in the atmosphere is an important storage and energy transfer medium of the global water household, influencing Earth's climate in many ways. Among the greenhouse gases water vapor holds an important and difficult status: On the one hand it enforces global warming acting as a filter of Earth's long wave radiation (albedo). On the other hand it can reduce the absorption of solar energy in form of clouds. The spatio-temporal distribution of water vapor in the troposphere (the neutral atmosphere) can be subject to rapid variations, and therefore, it is difficult to be measured and modeled. Vertical profiles of the partial pressure of water vapor in the troposphere can sparsely be measured by radiosondes. Observational techniques such as water vapor radiometer or solar spectrometer detect the characteristic absorption of water vapor, but are bound to good weather conditions, and the orbit of the sun, respectively. Therefore, we agree with Hagemann et al. [2003], that present observing systems are inadequate to monitor water vapor and its spatio-temporal distribution properly. Since it is questionable

whether climate trends can be calculated from reanalysis data [Bengtsson et al., 2004], such as the 40-years re-analysis product (ERA-40) of the European Centre of Medium-Range Weather Forecasts (ECMWF), the space-geodetic techniques, in particular Very Long Baseline Interferometry (VLBI), can give an important contribution to meteorological research.

In Section 2 we give a general introduction on the determination of water vapor.

Then we discuss our approach for the determination of trends and other signal components in Section 3. Due to VLBI's organizational and observational characteristics its time-series are usually irregularly sampled and clumped. Possible causes of a trend in time-series of precipitable water (*PW*) are considered and investigated in Section 4. Zenith wet delays (*ZWD*) for this study are taken from long time-series determined by several Analysis Centers (AC) of the International VLBI Service for Geodesy and Astrometry (IVS) [Schlüter et al., 2002] combined on the level of parameter estimates [Heinkelmann et al., 2007].

2. Determination of water vapor by space-geodetic techniques

The determination of water vapor by space-geodetic techniques operating on radio wavelengths, e.g. VLBI and Global Navigation Satellite Systems (GNSS), is based on the excess delay of radio signals traveling through the wet tropospheric medium and through the corresponding hydrostatic medium

$$\Delta L(E, A) = m f_h(E) \cdot ZHD + m f_w(E) \cdot ZWD + m f_g \cot(E) [G_N \cos(A) + G_E \sin(A)] \quad (1)$$

depending on elevation E (deg) and azimuth A (deg) angles of an observation. The total tropospheric delay in the line of sight ΔL (m) completely describes the effects of the tropospheric medium on VLBI observables. In Equation (1), the hydrostatic and wet mapping functions $m f_h$, $m f_w$ are assumed to be known and the gradient mapping function $m f_g$ is either the wet or the hydrostatic mapping function [MacMillan, 1995]. While ZWD (m) and the gradient components in north G_N (m) and east direction G_E (m) are estimated [Koch, 1997], zenith hydrostatic delays ZHD (m) can be computed by Davis et al. [1985]

$$ZHD = \frac{0,0022768 p}{1 - 0,00266 \cos(2\phi) - 0,00028h} \quad (2)$$

and are typically considered as corrections to the vector of observations. In Equation (2) the atmospheric surface pressure p (hPa), the latitude ϕ and height h (km) refer to the antenna reference point (ARP), i.e. the intersection of antenna axes of the VLBI telescope, or the antenna's phase center in the case of GNSS.

Following Bevis et al. [1993] the vertically integrated water vapor above the ARP can be expressed in terms of precipitable water PW (m) depending on the ZWD

$$PW = \Pi \cdot ZWD \quad (3)$$

where the factor Π is given by

$$\Pi = \frac{10^6}{\rho_l \cdot R_v [(k_3/T_m) + k'_2]} \quad (4)$$

In Equation (4) $\rho_l = 998.2$ (kg m⁻³) denotes the temperature-dependent density of liquid water at 20 (°C) and $R_v = 461.525$ (J kg⁻¹ K⁻¹)

denotes the specific gas constant of water vapor. The variables k'_2 and k_3 are refractivity constants and T_m is a weighted mean temperature of the atmosphere above the ARP. The correlation between T_m and the measured surface temperature T (K) was studied by Bevis et al. [1993], who analyzed two years of radiosonde observations over the United States territory. They found a linear relation: $T_m = 70.2 + 0.72T$.

3. Assessment of climate signals

In general, a climate signal y_t can be considered as linear combination of a constant mean, a trend component, one or more cycles, extreme events or outliers, and a noise component

$$y_t = \text{mean} + \text{trend} + \text{cycle} + \text{extrema} + \text{noise} \quad (5)$$

While the cyclic component consists of those parts of the signal, which are reproduced during certain periods, the trend component describes the temporal change of the signal in a non-cyclic sense. In general the trend component is not linear. Outliers can be identified either manually or automatically by applying robust estimation. The noise component is characterized by a zero expectation and a constant standard deviation. In our analysis we compare approximations of climate signals by two approaches: First we calculate and remove the mean value of the signal. Then we identify the periods of cycles by spectral analysis and determine the corresponding amplitudes and phases of sinusoids. In the sequel, we approximate the trend component by a simple linear term determined by robust regression. Alternatively we describe linear and non-linear characteristics of the trend by wavelet modeling.

3.1. Fourier expansion of cyclic components in ZWD time-series

Fig. 1 shows the spectra of ZWD at Gilmore Creek determined by three methods: the discrete Fourier transform, the Lomb-Scargle periodogram [Lomb, 1976], and the 'CLEANed-spectrum' obtained by the CLEAN-algorithm [Roberts et al., 1987]. The discrete Fourier spectrum shows peaks at periods >1 year, which are not significant in the spectra derived with the two other methods. Since the Lomb-Scargle periodogram and in particular the CLEAN-algorithm are designed to operate on unequally spaced data, we consider those periods to be artifacts due to the irregular sampling of the time-series. The discrete Fourier spectrum in addition shows some power along the shorter Fourier-periods (1/3 year, 1/4 year, etc.).

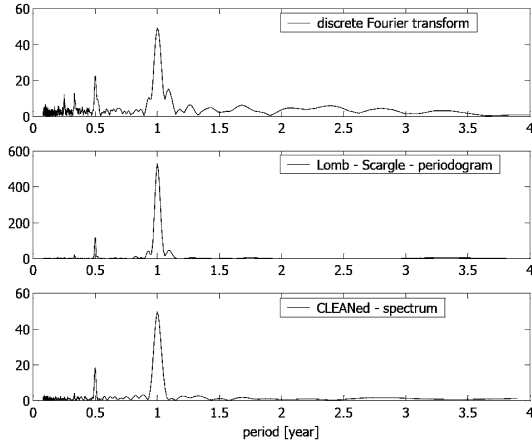


Figure 1: Three spectra of zenith wet delays (ZWD) at GILCREEK (Fairbanks, Alaska, USA) obtained by discrete Fourier transformation (top), Lomb-Scargle periodogram (mid), and CLEAN-algorithm (bottom). The abscissae give the amplitude (mm), or the power (mm²) in case of the Lomb-Scargle periodogram, and the ordinates the periods (years).

These shorter periods have no physical meaning, but are no artifacts as well. They emerge from the non-sinusoidal shape of the cyclic component. As a consequence annual, semi-annual and the next six periods are considered for the cyclic component.

$$y_t - \text{mean} = \text{cycle} + w_t$$

$$\text{cycle} = \sum_{i=1}^8 [A_i \sin(2\pi f_i t) + B_i \cos(2\pi f_i t)] \quad (6)$$

In Equation (6) A_i and B_i are the $i = 8$ pairs of coefficients characterizing amplitudes and phases of sinusoids with frequencies f_i corresponding to annual, semi-annual and 6 successive periods. The variable w_t denotes a residual signal, composed of *trend*, *extrema*, and *noise* components. After the f_i are identified from the spectra, the coefficients A_i and B_i of Equation (6) are determined by least-squares method; see e.g. Koch [1997].

3.2. Determination of linear trend by robust regression

After the cyclic component (Section 3.1) has been identified and removed, a linear trend can be estimated from the residual signal w_t , e.g. by robust estimation using the BIBER-estimator [Wicki, 2001]. However, in general, a climate trend is not fully described by a linear term and thus, it should not be modeled by a linear term only.

3.3. Trend approximation using normalized quadratic B-splines

Linear and non-linear characteristics of a climate trend can be assessed and represented by wavelet modeling. Therefore, we apply the normalized quadratic B-spline function as one dimensional scaling function. The normalized B-spline $N_{j,k}^d(x)$ of order d is defined recursively at equally spaced knots $t_0^j, t_1^j, \dots, t_{m_j+d}^j$ and represented in levels $j = 0, \dots, J$ of different resolutions [Schmidt, 2007] with $k = 0, \dots, m_j - 1$ and $m = 1, \dots, d$ as

$$N_{j,k}^m(x) = \frac{x - t_k^j}{t_{k+m}^j - t_k^j} N_{j,k}^{m-1}(x) + \frac{t_{k+m+1}^j - x}{t_{k+m+1}^j - t_{k+1}^j} N_{j,k+1}^{m-1}(x) \quad (7)$$

and with initial values

$$N_{j,k}^0(x) = \begin{cases} 1 & \text{if } t_k^j \leq x < t_{k+1}^j \\ 0 & \text{else} \end{cases}; \quad (8)$$

see e.g. Stollnitz et al. [1995]. In general, the B-spline of order d is compactly supported, i.e. its values are different from zero only in a finite range on the real axis. Since we want to use this approach for regional modeling we introduce the so-called endpoint-interpolated B-splines of order d defined on the unit interval $[0, 1]$.

For our investigations we choose with $d = 2$ the normalized quadratic B-spline functions $N_{j,k}^2(x)$. In this case the knot sequence is given as

$$0 = t_0^j = t_1^j = t_2^j < t_3^j < t_4^j < \dots < t_{m_j}^j = t_{m_j+1}^j = t_{m_j+2}^j = 1 \quad (9)$$

with $m_j = 2^j + 2$. Fig. 2 shows the normalized quadratic B-spline, for resolution level $j = 2$.

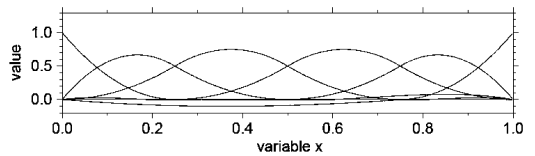


Figure 2: Normalized quadratic B-splines of resolution level.

Coefficients at the highest resolution level J are estimated by least-squares method, e.g. Koch [1997]. Then the coefficients related to the lower resolution levels $0 \leq j < J$ can successively be expressed by linear combinations starting from the highest level J . This so-called pyramid algorithm is the basic tool of the decomposition of the input signal into frequency-dependent detail signals, which is known as the multi-

resolution representation; see Schmidt [2007]. The level- j approximation means the sum of the detail signals until resolution level j . The highest resolution level J is implicitly given such that the relation $m_j = 2^J + 2 < n$ holds, where n denotes the number of observations.

When neglecting non-significant coefficients, the number of coefficients used for the representation of signals is reduced significantly. This can be interpreted as statistical data compression. The significance of the wavelet-coefficients can be assessed e.g. by hypothesis testing.

3.4. Comparison of the two approaches for the trend approximation

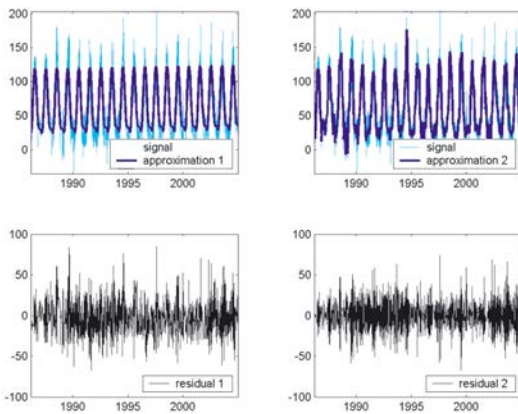


Figure 3: Zenith wet delays (ZWD) from International VLBI Service for Geodesy and Astrometry (IVS) combined series at GILCREEK (Fairbanks, Alaska, USA) between 1986.0 and 2005.0 (cyan). In blue approximation (1) by sinusoids, a linear and a constant term on the left ($\sigma = 20.7$ mm), as well as approximation (2) by sinusoids, B-spline wavelet modeling and a constant term on the right ($\sigma = 17.0$ mm). The corresponding residual signals are displayed in black (bottom). The abscissae give the ZWD (mm) and the ordinates the time (years).

Figure (3) exemplarily illustrates the ZWD for station Gilmore Creek in cyan (top). The blue curves display the two different approximations: On the left the trend component is modeled by a linear term only, while at the right side the trend component is represented by normalized quadratic B-splines until level $J = 7$. Cycles are considered by a Fourier expansion for both approaches. The rms of the noise component by modeling a linear trend only is 20.7 mm, whereas wavelet modeling yields a significantly smaller rms of 17.0 mm. Choosing a higher value for J the approximation can be improved.

4. Analysis of the trend component

Reconsidering Equations (1–7) a trend in time-series of PW will mainly be due to a trend of inherent ZWD . In addition, variations of wet and hydrostatic mapping functions and of ZHD , which mainly depend on the atmospheric pressure p , can affect the trend of PW . The temporal change of the proportionality factor Π due to the mean atmosphere temperature T_m and the density of liquid water ρ_l is of negligible size, i.e., the proportionality factor Π shows no significant variations itself. Trends in north and east gradients are typically of negligible size and do not have to be considered for the trend analysis of ZWD , or PW , respectively.

4.1. Atmospheric pressure

The atmospheric pressure is the mayor quantity for the determination of ZHD . Since ZHD are subtracted from the observations before the estimation of ZWD , inherent trends will propagate to the ZWD via the mapping functions. For most of the VLBI sites atmospheric pressure is automatically recorded in-situ, with a specific temporal resolution, and provided at the epoch of each observation. In-situ measurements are the source with the highest resolution. If outliers and missing values are appropriately replaced and significant shifts of the running mean are eliminated, in-situ atmospheric pressures are the most reliable pressure data. If in-situ atmospheric pressure data are not available, values should be taken from a numerical weather model (NWM). E.g. ERA-40, or operational data-sets of the ECMWF. If NWM are unavailable, we suggest the empirical global temperature and pressure (GPT) model [Böhm et al., 2007]. For the homogenization of in-situ atmospheric pressures as well as for the replacement of outliers and data gaps, the use of pressure time-series derived from NWM, such as the ERA-40, is very valuable and suggested by the authors. Significant shifts of the running mean of atmospheric pressure time-series recorded at VLBI stations [Heinkelmann et al., 2005] can be found by the application of a standard normal homogeneity test (SNHT) [e.g. Tuomenvirta and Alexandersson, 1996]. Shifts of the running mean of pressure time-series can be e.g. due to calibration, replacement, or relocation, in particular in height, of a pressure sensor. Figure (4) shows homogenized pressure time-series for station GILCREEK (Fairbanks, Alaska, USA) on the bottom, as well as ZHD on the top in cyan. An approximation by wavelet modeling is displayed in blue.

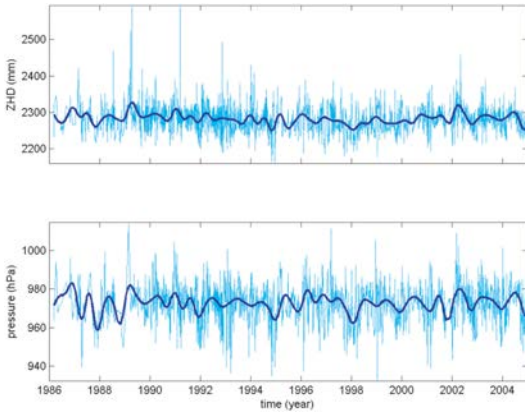


Figure 4: ZHD (top) from International VLBI Service for Geodesy and Astrometry (IVS) combined series at Gilmore Creek (Fairbanks, Alaska, USA) between 1986.0 and 2005.0 in mm and atmosphere pressure (bottom) in hPa are plotted in cyan. Approximations are displayed in blue.

4.2. Mapping functions

Trends in mapping functions directly and indirectly affect the trend of *ZWD*. The wet mapping function is the partial derivative of the observation with regards to *ZWD*. In addition the interdependency between *ZWD*, *ZHD* and the two gradient components are governed by the wet and hydrostatic mapping functions.

Various authors provide mapping functions by time-series of coefficients for particular stations or in form of global grids. Currently, the most accurate mapping functions globally available are the Vienna Mapping Functions 1 (VMF1) [Böhm et al., 2006]

$$mf(E) = \frac{1 + \frac{a}{1 + \frac{b}{1+c}}}{\sin(E) + \frac{a}{\sin(E) + \frac{b}{\sin(E)+c}}} \quad (10)$$

Here, wet and hydrostatic mapping functions *mf* are given by three coefficients *a*, *b*, *c*. The coefficients *a* are determined from raytracing through ECMWF data and are provided with a temporal resolution of *t* = 6 (hours). The coefficients *b* and *c* are calculated from empirical equations. The mapping functions depend on the elevation angle *E* of on observation and the latitude of a station. Figure (5) exemplarily displays the VMF1 at Gilmore Creek for an elevation angle of *E* = 5 (deg).

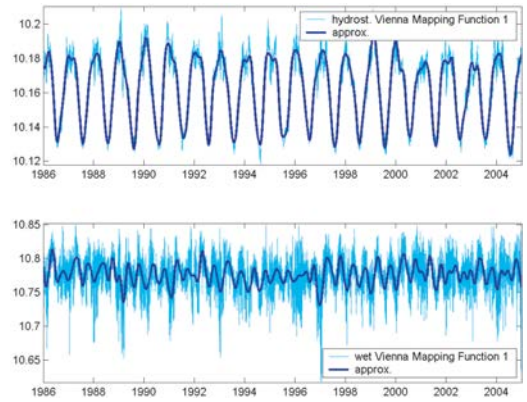


Figure 5: Hydrostatic (top) and wet (bottom) Vienna Mapping Functions 1 (VMF1) at Gilmore Creek (Fairbanks, Alaska, USA) for elevation angle *E* (deg) in cyan as well as approximations in blue. The abscissae give the unitless values of the mapping functions and the ordinates the time (years).

5. Results and discussion

VLBI is able to provide time-series of *ZWD*, which can be transformed to *PW*, i.e., high-quality information about the amount of water vapor above the VLBI stations.

If time-series of *ZWD*, or *PW*, are interpreted in terms of climate signals, the atmospheric pressure and mapping function time-series used for the determination of *ZWD* have to be considered. In particular the time-series of atmospheric pressure need to be homogenized, i.e. shifts of the running mean value due to sensor relocation, replacement, etc. need to be identified and removed. Trends in atmospheric pressure and mapping function time-series can cause apparent trends in *ZWD* (Equations 1 and 2).

Table 1 gives the linear trends determined by robust estimation (Section 3.2) for the twelve most frequently observing VLBI sites [Behrend and Bayer, 2005]. At some of those VLBI sites *ZWD* are available for more than 20 years. Thus, due to the large number of inherent *ZWD* estimates the formal errors of the linear trends are usually very small (see Table 1). However, the noise component dominates the climate signal. E.g. for the observed trend of 0.29 (mm/year) and the standard deviation of the noise component of 20.7 (mm) at station GILCREEK, the trend to noise ratio of ~0.014 indicates a very low significance of the trend. Instead of the formal errors of the linear trends, we suggest to consider the 1σ-level of the noise, to assess the significance of the trend.

station	time span	lin. trend (mm/year)	formal error (mm/year)	1- σ of the noise (mm)
ALGOPARK	1995–2005	−0.24	0.09	39.5
FORTLEZA	1995–2005	0.99	0.06	35.7
GILCREEK	1986–2006	0.29	0.01	20.7
HARTRAO	1993–2005	0.63	0.06	34.4
HOBART26	1993–2005	−0.31	0.06	31.1
KOKEE	1993–2005	0.78	0.04	33.7
MATERA	1993–2005	0.48	0.04	26.2
NYALES20	1995–2005	1.61	0.02	17.4
SESHAN25	1990–2005	−1.95	0.31	57.7
TSUKUB32	1997–2005	−2.33	0.22	51.2
WESTFORD	1986–2006	−0.15	0.07	47.4
WETTZELL	1986–2006	−0.07	0.02	20.2

Table 1: Linear trend estimates (mm/year) from International VLBI Service for Geodesy and Astrometry (IVS) combined series [Heinkelmann et al., 2007]

Comparison of linear trend estimates [Heinkelmann et al., 2007] shows better agreement of linear trends in case of synchronized data. This effect is probably also due to the large noise component.

In comparison to the linear trend model, the normalized quadratic B-spline wavelets appeared to be more capable of representing linear and non-linear characteristics of the trend component. E.g. at Gilmore Creek the sigma of the residuals drops from 20.7 (mm) to 17.0 (mm), if the trend component is modeled by a quadratic normalized B-spline of level $J = 7$, instead of a linear term only. In particular inter-annual variations of the amplitude of the seasonal signal are much better described by the wavelet model. In our example the variations of the annual amplitude of the seasonal signal at Gilmore Creek exceed the size of the linear trend by 1 to 2 orders of magnitude.

Acknowledgements

Many thanks to Claudia Zeilhofer (DGFI) for providing source code for the B-spline determination and wavelet-coefficient estimation. The authors acknowledge the IVS and its components, the ZAMG for providing access to the ECMWF data, and the Austrian Science Fund FWF (Project No. P16992-N10) for supporting this work.

References

- [1] Behrend D. and Baver K. (editors) [2005]: International VLBI Service for Geodesy and Astrometry. IVS Annual Report 2004, NASA/TP-2005-212772, NASA, Greenbelt
- [2] Bengtsson L., Hagemann S., Hodges K. I. [2004]: Can climate trends be calculated from reanalysis data? Journal of Geophysical Research. Vol. 109(D11111), doi:10.1029/2004JD004536
- [3] Bevis M., Businger S., Chiswell S., Herring T. A., Anthes R. A., Rocken C., Ware R. H. [1993]: GPS meteorology: mapping zenith wet delays onto precipitable water. Journal of Applied Meteorology. Vol. 33, 379-386
- [4] Böhm J., Heinkelmann R., Schuh H. [2007]: Short Note: A global model of pressure and temperature for geodetic application. Journal of Geodesy. doi:10.1007/s00190-007-0135-3
- [5] Böhm J., Werl B., Schuh H. [2006]: Troposphere mapping functions for GPS and very long baseline interferometry from European Centre for Medium-Range Weather Forecasts operational analysis data. Journal of Geophysical Research. Vol. 111, doi:10.1029/2005JB003629
- [6] Davis J. L., Herring T. A., Shapiro I. I., Rogers A. E. E., Elgered G. [1985]: Geodesy by radio interferometry: Effects of atmospheric modelling errors on estimates of baseline length. Radio Science. Vol. 20(6), 1593-1607
- [7] Hagemann S., Bengtsson L., Gendt G. [2003]: On the determination of atmospheric water vapor from GPS measurements. Journal of Geophysical Research. Vol. 108(D21), doi:10.1029/2002JD003235
- [8] Heinkelmann R., Böhm J., Schuh H. [2005]: Homogenization of surface pressure recordings and its impact on long-term series of VLBI tropospheric parameters. In: Proceedings of the 17th Working Meeting on European VLBI for Geodesy and Astrometry, Vennebusch M., Nothnagel A. (editors), INAF-Instituto di Radioastronomia-Sezione di NOTO, Italy, 74-78

- [9] Heinkelmann R., Böhm J., Schuh H., Bolotin S., Engelhardt G., MacMillan D. S., Negusini M., Skurikhina E., Tesmer V., Titov O. [2007]: Combination of long time-series of troposphere zenith delays observed by VLBI. *Journal of Geodesy*. doi:10.1007/s00190-007-0147-z
- [10] Koch K. R. [1997]: Parameterschätzung und Hypothesentests. 3rd edition. Dümmler, Bonn, 368
- [11] Lomb N. R. [1976]: Least-squares frequency analysis of unequally spaced data, *Astrophysics and Space Science*. Vol. 39, 447-462
- [12] MacMillan D. S. [1995]: Atmospheric gradients from very long baseline interferometry observations. *Geophysical Research Letters*. Vol. 22(9), 1041-1044
- [13] Roberts D. H., Lehar J., Dreher J. W. [1987]: Time series analysis with CLEAN. I. Derivation of a spectrum. *Astronomical Journal*. Vol. 93(4), 968-989
- [14] Schlüter W., Himwich E., Nothnagel A., Vandenberg N., Whitney A. [2002]: IVS and its important role in the maintenance of the global reference systems. *Advances in Space Research*. Vol. 30(2), 145-150
- [15] Schmidt, M. [2007]: Wavelet modelling in support of IRI. *Advances in Space Research*. doi:10.1016/j.asr.2006.09.030
- [16] Stollnitz E. J., DeRose T. D., Salesin D. H. [1995]: Wavelets for Computer Graphics: A Primer. Institute of Electrical and Electronics Engineering - Computer Graphics and Applications. Vol. 15(3), 76-84 (part 1), and Vol. 15(4), 75-85 (part 2)
- [17] Tuomenvirta H., Alexandersson H. [1996]: Review on the methodology of the standard normal homogeneity test (SNHT). In: Proceedings of the 1st seminar for homogenization of surface climatological data, Hungarian Meteorological Service (editors), 35-45
- [18] Wicki F. [2001]: Robust estimator for the adjustment of geodetic networks. In: Proceedings of the 1st international symposium on robust statistics and fuzzy techniques in geodesy and GIS. Carosio A. and Kutterer H. (editors), International Association of Geodesy – Special Study Group 4.190. Non-probabilistic assessment in geodetic data analysis, Swiss Federal Institute of Technology Zurich (ETH). Institute of Geodesy and Photogrammetry. IGP – Bericht Nr. 295, 53-60

Contact

Dipl.-Ing. Robert Heinkelmann, Institute of Geodesy and Geophysics, Vienna University of Technology, Gusshausstr. 27-29, A – 1040 Vienna, Austria.

E-mail: rob@mars.hg.tuwien.ac.at

PD Dr.-Ing. habil. Michael Schmidt, Deutsches Geodätisches Forschungsinstitut, Alfons-Goppel-Str. 11, D – 80539 Munich, Germany. E-mail: schmidt@dgfi.badw.de

Dr. Johannes Böhm, Institute of Geodesy and Geophysics, Vienna University of Technology, Gusshausstr. 27-29, A – 1040 Vienna, Austria.

E-mail: johannes.boehm@tuwien.ac.at

Prof. Dr. Harald Schuh, Institute of Geodesy and Geophysics, Vienna University of Technology, Gusshausstr. 27-29, A – 1040 Vienna, Austria.

E-mail: harald.schuh@tuwien.ac.at